# Effective Transport Template for Particle Separation in Microfluidic Bumper Arrays

Stefano CERBELLI[1,*], Fabio GAROFALO[2] and Massimiliano GIONA[1]

[*] Corresponding author: stefano.cerbelli@uniroma1.it
[1] Dept. of Chemical Engineering, University of Rome "La Sapienza", IT
[2] Dept. of Mechanical Engineering, Technical University of Eindhoven, NL

**Abstract.** Microfluidic bumper arrays are increasingly being used for the size-based sorting of particle suspensions. The separation mechanism is based on the interaction between a spatially periodic array of obstacles and the suspended particles as they are driven through the obstacle lattice either by volume forces or by the Stokesian drag of the surrounding fluid. By this mechanism, a focused stream of suspended particles of different sizes entering the lattice splits into different currents, each entraining assigned ranges of particle dimensions, and each characterized by a specific angle with respect to the main device axis. In this work, we build up on recent results stemming from macrotransport process theory to derive a closed-form solution for the steady-state distribution of advecting-diffusing particles in the presence of anisotropic dispersion, which typically characterizes large-scale behavior of particle motion through the periodic lattice. Attention is focused on separation resolution, that ultimately controls the feasibility of the separation in specific applications.

**Keywords:** Particle Sorting, Effective Dispersion, Separation Resolution

## 1. Introduction

As micro-fabrication techniques make it possible to produce micrometer-sized geometries with unprecedented resolution, an increasing number of prototypes are being continuously proposed, which realize classical engineering operations based on altogether new design principles. The separation method referred to as Deterministic Lateral Displacement (Huang et al., 2004) constitutes one such example, where an elegant use of simple fluid dynamic ideas allows to perform in an efficient way the size-based separation of a multidisperse population of micrometer-sized objects suspended in a carrier fluid, be them solid particles, bacteria, or even drops of an immiscible phase (Devendra & Drazer, 2012; Holm et al, 2011; Green et al., 2009). A typical realization of a device exploiting this principle is constituted by a shallow rectangular channel filled with a periodically ordered array of identical obstacles arranged along a Cartesian lattice. The lattice is given an angle, say $\Theta_l$ , with respect to the lateral walls of the channel. A pressure-driven flow, entraining the multidisperse suspension, crosses the array of impermeable obstacles. The geometry is designed so that the typical size of the objects in the mixture is comparable to the gap between adjacent obstacles. Figure 1 provides a schematic representation of the separation mechanism for the case where the lattice angle is given by $\Theta_l = 1/3$. The red thick lines represent critical streamlines of the Stokes flow through the periodic array of obstacles. These critical streamlines define flux tubes that extend throughout the domain. The separation mechanism can be explained by assuming that a generic finite-sized particle is constrained to follow the streamline

through its center until it comes into contact with an obstacle. At the collision, the particle starts to glide around the obstacle and eventually detaches from it by following a different streamline. According to this simplified model, one observes two qualitatively different behaviors of particle dynamics: small particles tend to remain constrained within a single flux tube (zig-zag mode), whereas larger particles change flux tube at each collision with an obstacle (displacement mode).

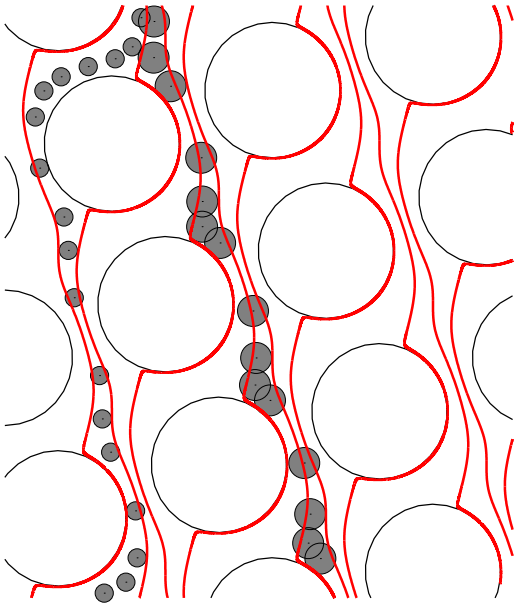

Figure 1: Critical streamlines of the single phase Stokes flow through a tilted periodic array of cylindrical obstacles (thick red lines). The gray circles display the paths of finite-sized particles dragged by the surrounding fluid through the obstacle lattice.

The critical particle size separating the two separation modes is given by the condition that the particle radius be equal the the minimal width of the flux tube immediately adjacent to any given obstacle. A number of experiments involving solid-particle or even cell suspensions, provided a qualitative validation of this simple interpretation scheme for the separation mechanism, even though it has been recognized that the impact of thermal fluctuations on separation efficiency should not be neglected if an accurate design of the separation device is sought (Heller & Bruus, 2008). More recent work (Cerbelli et al., 2013; Cerbelli 2013) has showed how the superposition of thermal fluctuations to the simple kinematic scheme described above can have a significant influence not only on the average direction attained by particles of a given size, but also on the dispersion of individual particles about the average particle current. It has been found that enhanced dispersion regimes, hindering separation efficiency far beyond what could be predicted from the value of bare particle diffusivity, can arise as a consequence of the interaction between thermal fluctuations and flow structure. The scope of this work is to analyze the practical consequences of these dispersion regimes in device geometries and operating conditions that are typically used in practical implementations of this separation technique. Specifically, we derive the analytical solution of the steady-state particle number density associated with a localized continuous feeding of the particle suspension, which closely mimics the typical setting of practical implementations of the separation method. We expect the conclusions of this analysis to be especially relevant for possible further scale-down of this process to the separation of mesoscopic objects in the range of hundreds of nanometers, a domain of lengthscales where thermal fluctuations cannot be overlooked.

## 2. Transport model and macroscale dispersion

In what follows, we consider transport and dispersion of neutrally buoyant spherical particles suspended in a Newtonian fluid flowing in the Stokes regime through a bi-periodic lattice of cylindrical obstacles, such as that depicted in Fig. 2.

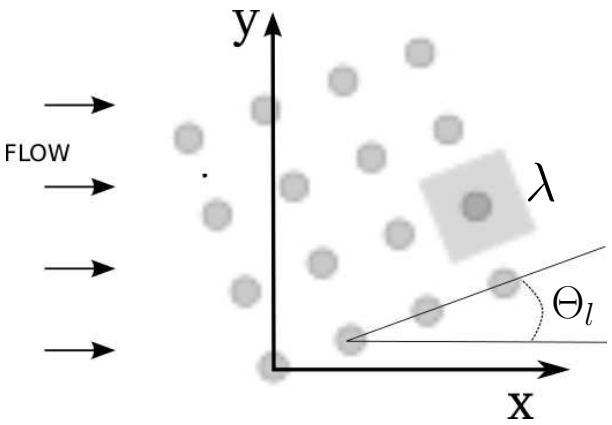


Figure 2: Global reference frame for a tilted lattice of cylindrical obstacles at an angle $\Theta_l$ with the average direction of the carrier flow. The gray-shaded area represent the elementary cell of the periodic lattice.

The $x$-axis of the global coordinate frame is taken collinear with the average flow velocity, and the smallest angle between the principal lattice directions and the flow direction is denoted as the lattice angle $\Theta_l$. As the carried fluid flows through the lattice of obstacles, a generic suspended particle is subjected to three main actions, namely -(i) the Stokesian drag of the surrounding fluid, -(ii) the action of the obstacles, and -(iii) the thermal (stochastic) fluctuations. Because the particle radius, say $a$, is of order of $1\,\mu m$, particle inertia can be neglected and the overdamped regime can be assumed. By these hypothesis the microscale advection-diffusion process can be modeled by the stochastic differential equations

$$\begin{aligned} dx &= (u - \partial_x V)\; dt + \sqrt{2/\mathrm{Pe}}\; d\xi_1 \\ dy &= (v - \partial_y V)\; dt + \sqrt{2/\mathrm{Pe}}\; d\xi_2 \end{aligned} \qquad (1)$$

where $x, y$ denote the dimensionless coordinate of the center of the particle, $u = u(x, y)$, $v = u(x, y)$ are the dimensionless components of the unperturbed fluid velocity at the particle center, $V = V(x, y)$ represent the dimensionless potential that expresses the interaction between the particle and the obstacle lattice (Frechette & Drazer, 2009) , $d\xi_1$ $d\xi_2$ represent independent Wiener process with zero mean and unit variance, $Pe = U\lambda/\mathcal{D}$ is the particle Peclet number, $U$, $\lambda$, and $\mathcal{D}$ being a reference velocity, a reference length, and the particle diffusivity, respectively (see Cerbelli et al., 2013 for details). The particle diffusivity can be estimated by the Stokes-Einstein relationship $\mathcal{D} = k_b\, T/(6\,\pi a \mu)$, where $k_b$ is the Boltzmann constant and $\mu$ the dynamic viscosity of the carrier fluid. One may choose $U$ equal to the average velocity of the carrier flow, and $\lambda$ equal to the size of the unit cell of the lattice (see Fig. 2).

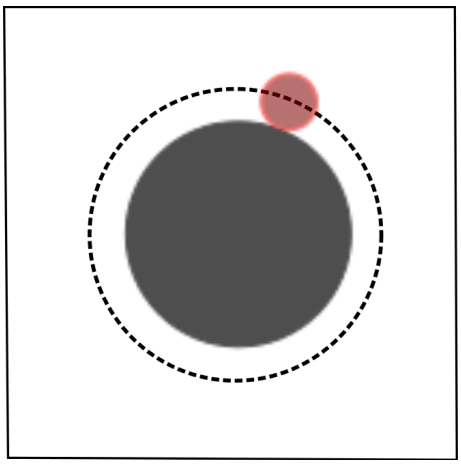

Figure 3: Effective obstacle model. The gray-shaded area represents the physical obstacle, the dashed line depicts the effective obstacle size defining the portion of the flow domain that is accessible to the center of the finite-sized particle (red circle).

Note that the specific structure of the doubly-periodic potential landscape depends on the particle radius, meaning that the *potential gradient must become singular whenever the distance between the center of the particle and the center of the obstacle approaches the sum of the particle and the obstacle radius*. Recently, a simple model of obstacle-particle interaction has been proposed (Cerbelli et al. 2013, Cerbelli, 2013) where the obstacle potential possesses a singular step-wise structure. This means that the particle is unaffected

by the presence of the obstacles, until its center comes to a distance equal $a$ from the obstacle boundary, where the action of the obstacle is such as to annihilate the component of the particle velocity normal to its boundary. This implies that the particle can be regarded as a point tracer (ideally collapsed at its geometric center) which - unlike fluid elements - is allowed to move through a lattice of *effective obstacles*, whose size equals that of the physical obstacles plus the particle radius. Eulerian and Lagrangian approaches proved that at spatial scales much larger than the cell size $\lambda$, and at times $t$ much larger than the characteristic convective time over the cell size, the particle number density $\phi(X, Y, t)$ of an ensemble of tracers evolving under the microscale process Eq. (1) is governed by the effective dispersion equation

$$\partial_t \phi + \mathbf{v} \cdot \nabla_{\mathbf{X}} \phi = \nabla_{\mathbf{X}} \cdot \big( \mathbb{D} \cdot \nabla_{\mathbf{X}} \phi \big), \quad (2)$$

$\mathbf{v}$ is a constant effective particle velocity, $\mathbb{D}$ is a *generally non-isotropic, positive-definite effective diffusivity tensor,* $\mathbb{D} = ((D_{ij}))$, and where $\nabla_{\mathbf{X}}$ denotes differentiation w.r.t. the large scale coordinates $\mathbf{X} = (X, Y)$, where $X, Y >> \lambda$. Because the direction associated with the average particle velocity depends on $a$, particle of different radii follow on the average different deflection angles, thus making it possible to sort particles based on their size. Figure 4 provides and illustrative example of the collective behavior of a mixture of particles of two characteristic sizes, all initially located at the origin of the coordinate system. As time goes by, the center of mass $\mathbf{x}_c(t)$ of the evolving swarm moves according to $\mathbf{x}_c(t) = \mathbf{v}\, t$, whereas the dispersion of the individual particles about the average motion is quantified by an ellipsoid, whose principal axes are typically at an angle with both the direction of the carrier flow, and the average particle velocity $\mathbf{v}$. The ellipsoid axes are given by the principal directions of the effective diffusivity tensor $\mathbb{D}$, whereas the characteristic dispersion lengths $\Sigma_1$, $\Sigma_2$ along these directions grow as $\Sigma_1^2 = 2\, D_1 t$, $\Sigma_2^2 = 2\, D_2 t$, where the principal dispersion coefficients $D_1$ and $D_2$ are the eigenvalues of $\mathbb{D}$ (see Fig. 5).

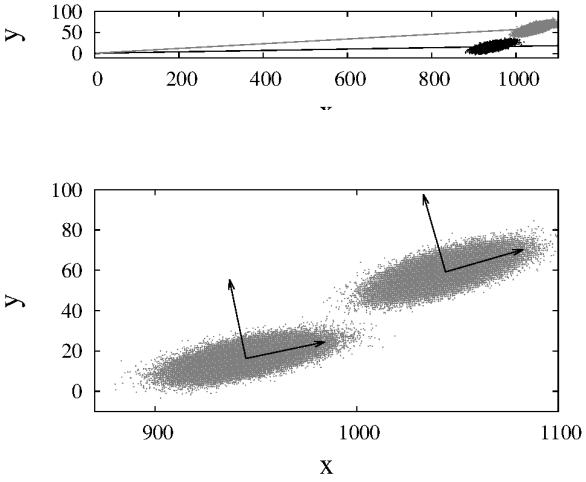


Figure 4: Upper panel: Large-scale dispersion for an impulsive initial condition centered at the origin in a squared tilted lattice $\Theta_l = \tan^{-1}(1/10)$ The black and gray clouds represent particle of different sizes. The continuous lines represent the position of the center of mass of the ensemble as time goes by. Panel B: Zoom-in of the particle ensembles showing the principal axes of the effective dispersion tensor.

From a phenomenological standpoint, it has been found that both the principal diffusivities and the angle $\Theta_D$ defining the principal directions (Fig. 5) depend strongly on the particle Peclet number $Pe$. Specifically it has been observed that the principal diffusivities display an enhanced dispersion scaling $D_1 \simeq Pe^{-\alpha_1}$, $D_2 \simeq Pe^{-\alpha_2}$, where $0 \leq \alpha_i \leq 1$ $(i = 1, 2)$, the two power-law exponents being typically unequal. For comparison, one notes that in this dimensionless formulation, an ensemble of particles evolving in a uniform flow (i.e. with $u$, $v$ and $V$ constant in Eq. 1) would be characterized by an isotropic effective dispersion tensor given

by $\mathbb{D} = (1/Pe)\,\mathbb{I}$ where $\mathbb{I}$ is the identity tensor.

A logarithmic scaling $D \simeq A/(B + \ln Pe)$ has also been observed and theoretically justified for particle sizes near critical values separating different kinematic modes along the direction orthogonal to the average velocity of the carrier flow (Cerbelli, 2013).

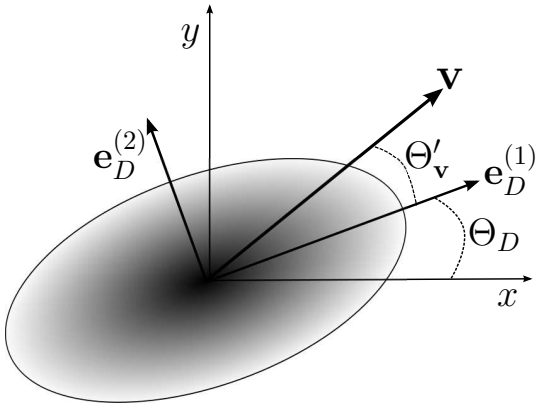


Figure 5: Geometric representation of the parameters defining the effective transport model. The grey-shaded area represents the dispersion ellipsoid, $\mathbf{e}_D^{(1)}$, $\mathbf{e}_D^{(2)}$ its principal directions corresponding to the dispersion coefficients $D_1$, $D_2$, $\mathbf{v}$ is the large-scale average particle velocity.

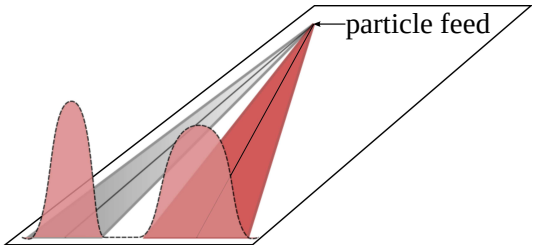


Figure 6: Schematic representation of separation for a mixture of suspended particles of two different sizes in a Deterministic Lateral Displacement device. The solid lines represent the average particle path. The shaded angles depict the broadening of the particle currents downstream the device.

In the next Section, we develop a closed-form model for predicting the particle density profile at the outlet cross-section of a deterministic lateral displacement device based on the effective transport parameters $\mathbf{v}$ and $\mathbb{D}$

## 2. Dispersion from a continuous localized source

When discussing the large-scale features of particle dispersion associated with the model expressed by Eq. (1), we focused on the collective behavior of an ensemble of particles all released instantaneously at $t = 0$ at one and the same spatial location, which was assumed to be the origin of the global coordinate system. However, in a real separation experiment, particles are released continuously from a feeding micro-channel at a given point of the inlet cross-section (see Fig. 6). Therefore the particle number density function that describes the steady-state dispersion process in the large-scale long-time limit is given by the solution to the stationary effective transport problem

$$\mathbf{v} \cdot \nabla_{\mathbf{X}} \phi = \nabla_{\mathbf{X}} \cdot \big(\mathbb{D} \cdot \nabla_{\mathbf{X}} \phi\big) + \delta(\mathbf{X}), \qquad (3)$$

where the Dirac's function at the right hand side of Eq. (3) represents a (normalized) continuous feeding at the origin of the global coordinate system, and where it is henceforth assumed that the all the variables are made dimensionless by taking the cell size $\lambda$ and the average particle velocity, say $W$, as fundamental reference quantities (i.e. $\|\mathbf{v}\| = 1$). The solution to this transport problem is best worked out in an orthogonal reference frame - still centered at the origin of the $xy$ axes - whose axes, say $\xi_1$, $\xi_2$,, are collinear with the principal directions $\mathbf{e}_D^{(1)}$, $\mathbf{e}_D^{(2)}$ of the effective dispersion tensor depicted in Fig. 5. In this frame, the (dimensionless) steady-state transport problem writes

$$\begin{aligned} &\cos\Theta'_{\mathbf{v}}\,\partial_{\xi_1}\Phi + \sin\Theta'_{\mathbf{v}}\,\partial_{\xi_2}\Phi = \\ &D_1\,\partial^2_{\xi_1\,\xi_1}\Phi + D_2\,\partial^2_{\xi_2\,\xi_2}\Phi + \delta(\xi_1,\xi_2) \end{aligned} \qquad (4)$$

The solution $\Phi(\xi_1,\xi_2) = \phi\big(\xi_1(x,y),\xi_2(x,y)\big)$ to this problem can be expressed in terms of the

Green function $\mathcal{G}(\xi_1, \xi_2, t)$ associated with the transient dispersion problem Eq. (2) written in the $\xi_1, \xi_2$ coordinates,

$$\mathcal{G}(\xi_1, \xi_2, t) = F(t)\; e^{-\frac{(\xi_1 - v_1' t)^2}{4 D_1 t} - \frac{(\xi_2 - v_2' t)^2}{4 D_2 t}} \qquad (5)$$

where $F(t) = 1/(4\pi\, t\, \sqrt{D_1 D_2})$, $v_1' = \cos\Theta_{\mathbf{v}}'$, and $v_2' = \sin\Theta_{\mathbf{v}}'$ (see Fig. 5 for the definition of $\Theta_{\mathbf{v}}'$). The steady-state solution can be expressed as

$$\Phi(\xi_1, \xi_2) = \int_0^\infty \mathcal{G}(\xi_1, \xi_2, t)\; dt \qquad (6)$$

By defining

$$\begin{aligned} a(\xi_1, \xi_2) &= \tfrac{\xi_1^2}{4\, D_1} + \tfrac{\xi_2^2}{4\, D_2} \\ b(\xi_1, \xi_2) &= \tfrac{\cos\Theta_{\mathbf{v}}'\, \xi_1}{2\, D_1} + \tfrac{\sin\Theta_{\mathbf{v}}'\, \xi_2}{2\, D_2} \qquad (7) \\ c = \text{const.} &= \tfrac{\cos^2\Theta_{\mathbf{v}}'}{4\, D_1} + \tfrac{\sin^2\Theta_{\mathbf{v}}'}{4\, D_2} \end{aligned}$$

the steady-state particle density profile can be expressed as

$$\Phi(\xi_1, \xi_2) = 2\, A\, e^{b(\xi_1, \xi_2)} K_0\big(2\, \sqrt{c\, a(\xi_1, \xi_2)}\big) \qquad (8)$$

where $A = 1/(4\pi\sqrt{D_1 D_2})$ and where $K_0(\eta)$ is the modified Bessel function of order zero, which is obtained by substituting Eq. (5) into Eq. (6). Figure 7 shows the short-range structure of the steady-state particle distribution near the localized feed, for a generic case where $\Theta_D$ and $\Theta_{\mathbf{v}}$ are different from zero. In this range, the normalized particle density profiles computed with respect to the $xy$-coordinates at constant $\overline{x}$,

$$\Phi_\nu(\overline{x}, y) = \frac{\Phi(\xi_1(\overline{x}, y), \xi_2(\overline{x}, y))}{\int_{-\infty}^{\infty} \Phi(\xi_1(\overline{x}, y), \xi_2(\overline{x}, y))\; dy} \qquad (9)$$

possess strongly asymmetric structure (see lower panel of Figure 7). This asymmetry is progressively lost when moving downstream the device, as showed in Fig. 8. At these spatial scales, the maximum of the distribution is attained at the average value $y_c$ given by

$$y_c(x) = \int_{-\infty}^{\infty} y\, \Phi_\nu(x, y)\; dy = x\, \tan\Theta_v\,, \qquad (10)$$

where $\Theta_{\mathbf{v}} = \Theta_{\mathbf{v}}' + \Theta_D$.

An interesting point is to determine the rate of growth of the variance

$$\sigma^2(x) = \int_{-\infty}^{\infty} \big(y - y_c\big)^2\, \Phi_\nu(x, y)\; dy \qquad (11)$$

along the downstream global coordinate $x$, in that this is the primary quantity that controls the separation resolution. Figure 9 shows $\sigma(x)$ for the particle mixture defined by the parameters of Fig. 8. At dimensionless distances $x > 10$ from the localized source, the variance associated both average particle velocities settles onto a power-law scaling (note that the scale of the figure is logarithmic), i.e. according to $\sigma(x) = \sqrt{2\, D_{\text{eff}} x}$ where $D_{\text{eff}}$ is an effective dispersion coefficient, thus indicating that the separation of the two species can always be accomplished even in the presence of diffusion, provided that the device is long enough as to avoid significant overlapping of the particle density profiles at the exit cross-section. The dotted lines in the same figure depict the scaling $\sigma(x) = \sqrt{2\, D_{\text{eff}} x}$ with $D_{\text{eff}} = \big(D_1 \sin\Theta_{\mathbf{v}}' + D_2 \sin\Theta_{\mathbf{v}}'\big)/\cos^3\Theta_{\mathbf{v}}$. Owing to space constraints, we postpone to future work the discussion about the range of validity of this simplified estimate. For the time being, we only highlight how the closed-form solution to the steady-state macrotransport model provides a useful framework for interpreting experimental results. Also, the knowledge of the solution can provide a guidance to design tailored experiments to untangle the intrinsic transport parameters $\Theta_{\mathbf{v}}$, $\Theta_D$, $D_1$, and $D_2$ from direct measures of particle number density profiles.

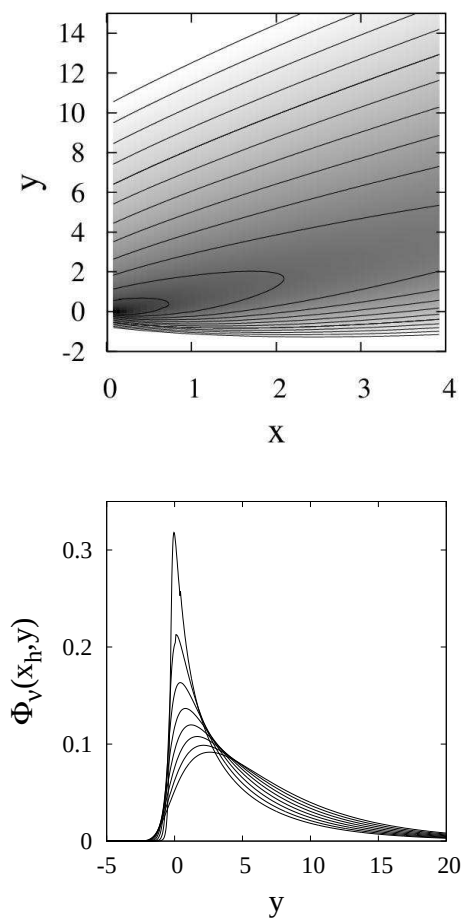


Figure 7: Upper panel: Short-range structure of the steady-state dimensionless particle number density for a continuous localized feed located at the origin with $\Theta_v = \Theta'_v + \Theta_D = \pi/4$, $\Theta_D = \pi/3$, $D_1 = 10^{-1}$, $D_2 = 1$. Contour levels span the interval $10^{-3} \leq \phi(x,y) \leq 1$. Lower panel: Normalized particle density profile along vertical lines at $x_h = 1/2; 1; 3/2; 2; 5/2; 3; 7/2; 4$ for the case depicted in the upper panel.

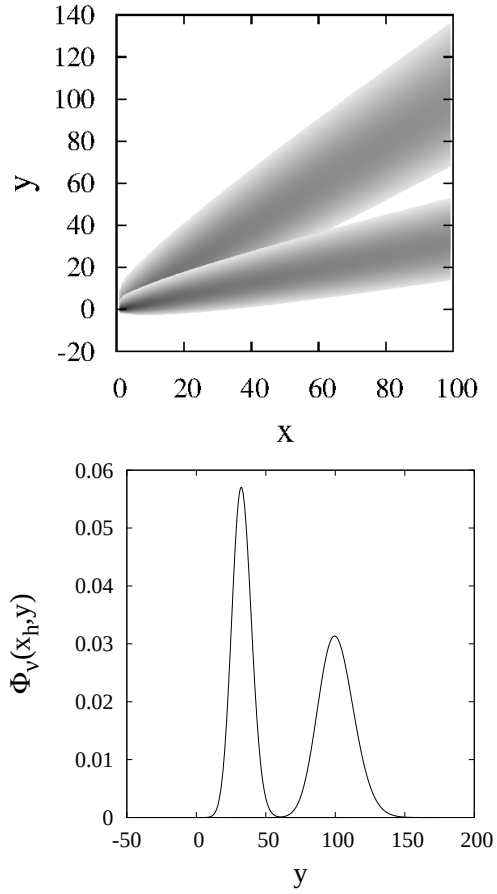


Figure 8: Upper panel: Long-range structure of the steady-state dimensionless particle number density for a continuous localized source located at the origin associated with different average velocities, $\Theta_v = \pi/10$, and $\Theta_v = \pi/4$. For both cases, $D_1 = 0.1$, $D_2 = 3\,D_1$, $\Theta_D = \pi/3$. The contour levels span the interval $(10^{-3}, 1)$ in a logarithmic scale. Lower panel: Normalized particle density profile along a vertical line at $x_h = 100$ for the case depicted in the upper panel.

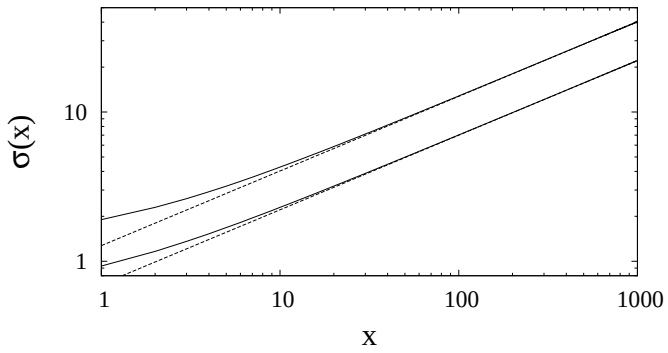


Figure 9: Variance of the normalized profiles downstream the direction of the carrier flow. At large distances from the localized particle source, the variance grows as $\sqrt{2\,D_{\rm eff}x}$.

## References

Cerbelli, S., Giona, M., Garofalo, F., 2013. Quantifying dispersion of finite-sized particles in deterministic lateral displacement microflow separators through Brenner's macrotransport paradigm. Microfl. Nanofl., 15, 431-449.

Cerbelli, S., 2013. Critical dispersion of advecting-diffusing tracers in periodic landscapes of hard-wall symmetric potentials. Phys. Rev. E (R), 87, 060102.

Frechette, J., Drazer, G., 2009. Directional locking and deterministic separation in periodic arrays. J. Fluid Mech., 627, 379-401.

Devendra, R., Drazer, G, 2012. Gravity driven deterministic lateral displacement for particle Separation in Microfluidic Devices. Anal. Chem, 84, 10621-10627.

Green, J.V. and Radisic, M. and Murthy, S.K., 2009. Deterministic lateral displacement as a means to enrich large cells for tissue engineering. Anal. Chem., 21, 9178-9182.

Heller, M., Bruus, H., 2008. A theoretical analysis of the resolution due to diffusion and size dispersion of particles in deterministic lateral displacement devices. J. Micromech. Microeng, 18, 075030

Holm, S.H. and Beech, J.P. and Barrett, M.P. and Tegenfeldt, J.O., 2011. Separation of parasites from human blood using deterministic lateral displacement. Lab on a Chip, 11, 1326-1332.

Huang, L.R., Cox, E.C., Austin, R.H., Sturm, J.C., 2004. Continuous particle separation through deterministic lateral displacement. Science, 304, 987-990.